AIAA 80-1417R

Low Reynolds Number Aerodynamic Characteristics of Low-Drag NACA 63-208 Airfoil

H.T. Nagamatsu*
Rensselaer Polytechnic Institute, Troy, N.Y.
and
D.E. Cuche†
Swiss Federal Institute of Technology, Zurich, Switzerland

An investigation was conducted to study the flowfield and the aerodynamic characteristics of a low-drag NACA 63-208 airfoil section over a low Reynolds number range of 35,400 to 176,500. The pressure measurements for the airfoil section were conducted for an angle-of-attack range of −17 to +18 deg in the low-speed wind tunnel. The pressure distribution was found to be quite different for various Reynolds numbers, but the maximum lift coefficient was nearly independent of the Reynolds number. At low Reynolds numbers, the slope of the pitching moment coefficient varied drastically with the angle of attack.

Introduction

AN investigation was initiated to study the flowfield and the aerodynamic characteristics of low-drag airfoil sections at a very low Reynolds number range of 20,000 to 500,000. The stall speed and the control and stability characteristics for flight vehicles at low Reynolds number depend on the maximum lift coefficient and the pitching moment of the airfoil sections. Low Reynolds number conditions exist for gliders at low speeds, remotely piloted vehicles, and first-stage compressors for jet engines at high altitudes.

Only limited characteristics at very low Reynolds numbers are available in the literature. The investigations conducted by NASA and other groups all over the world on the low Reynolds number airfoil phenomena at a Reynolds number range of 0.5 to 20 million are summarized in Refs. 1-10. Gault[6] studied the correlation of the low-speed airfoil stalling characteristics with Reynolds number and geometry. He concluded that for a Reynolds number of 0.7×10^6 there exists mainly a thin airfoil type of stall. Kelling[11] investigated the GU 25-5 airfoil at a Reynolds number of one-half million, and with a high-lift device, a $C_{L_{max}}$ of 1.93 was achieved.

In 1938 Pinkerton[12] published information on the variation of the pressure distribution over an NACA 4412 profile with Reynolds number at low subsonic speeds. The Reynolds number varied from 1×10^6 to 8.2×10^6 and the angle-of-attack range of −17 to +18 deg. The results indicated a strong dependence of the pressure distribution on the Reynolds number. Nakamura et al.[13] studied an NACA 0012 airfoil for a Reynolds number range of 30,000 to 280,000.

They observed that the stalling characteristics of the airfoil at low Reynolds numbers with the separation bubble extending 10-20% of the chord were quite different than at higher Reynolds numbers with a shorter extent of the bubble. Tani[14] investigated the low-speed flow involving bubble separation over an airfoil at an angle of attack for a Reynolds number of 1 million.

In the present investigation, a low-speed wind tunnel was calibrated before the testing of an NACA 63-208 airfoil section. This profile was selected for the following reasons:

1) Studies have been conducted in general for the 12% thick airfoils, NACA 4412 (Ref. 12), and NACA 0012 (Ref. 13).

2) The accurate airfoil section with the static pressure taps was loaned to Rensselaer Polytechnic Institute by the NASA Langley Research Center for the purpose of obtaining information at low Reynolds numbers. The airfoil was tested over a Reynolds number range of 35,400 to 176,500, where there is no available aerodynamic data for the selected airfoil.

Experimental Equipment and Procedure

Low-Speed Wind Tunnel

All of the tests were conducted in a small, closed-circuit wind tunnel, Fig. 1, with a length of 21 ft and a height of 10 ft. The test section, 18×27 in., has transparent side walls which permit a good view of the model for observing the tufts for stall condition. A dc electric motor allows a smooth and precise setting of the flow velocity in the 16-100 ft/s range. The top side of the test section is removable for installing the models. A screen is mounted ahead of the test section in the settling chamber to reduce the turbulence level and to make the velocity distribution across the test section nearly uniform, as discussed in Ref. 15.

Model

An NACA 63-208 airfoil wing with a span of 6 in. and a chord of 4 in. was loaned by NASA Langley Research Center to conduct the aerodynamic studies at very low Reynolds number below 1 million since no information was available. The model is constructed of steel with 21 pressure orifices located on the upper and lower surfaces as shown in Fig. 2.

Since the airfoil section was constructed for the NASA 6-in.-wide transonic wind tunnel, an extension was installed to support the model in the 18-in. high test section as shown in Fig. 3. Two end plates were installed to make the flow over the wing nearly two dimensional. The complete model was attached to a circular plate on the wind tunnel top surface for setting the angle of attack, and the other end was attached to a circular plate mounted on a pivot at the center.

Instrumentation

To measure the static pressures on the model, 3-ft long plastic tubes were attached to the static pressure tubes extending beyond the end plates as shown in Fig. 3. These plastic tubings were connected to four rotatable selector valves, which were connected to a micromanometer to measure the static pressures. The low-speed tunnel was continuously operated to obtain the static pressure distributions at various velocities and angles of attack.

A small pitot-static tube was used to survey the flow velocity distribution across the test section for different

Presented as Paper 80-1417 at the AIAA 13th Fluid and Plasma Dynamics Conference, Snowmass, Colo., July 14-16, 1980; received Aug. 6, 1980; revision received March 30, 1981.

*Professor, Aeronautical Engineering.
†Graduate Student.

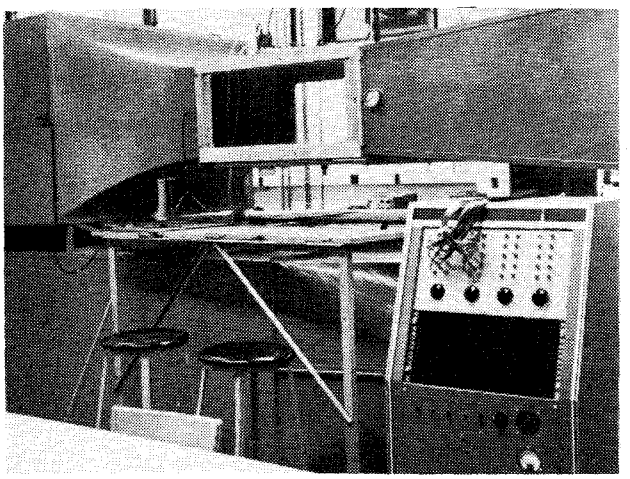

Fig. 1 Low-speed wind tunnel.

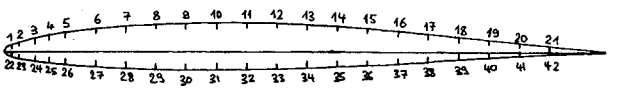

Fig. 2 NACA 63-208 airfoil section; location of pressure taps.

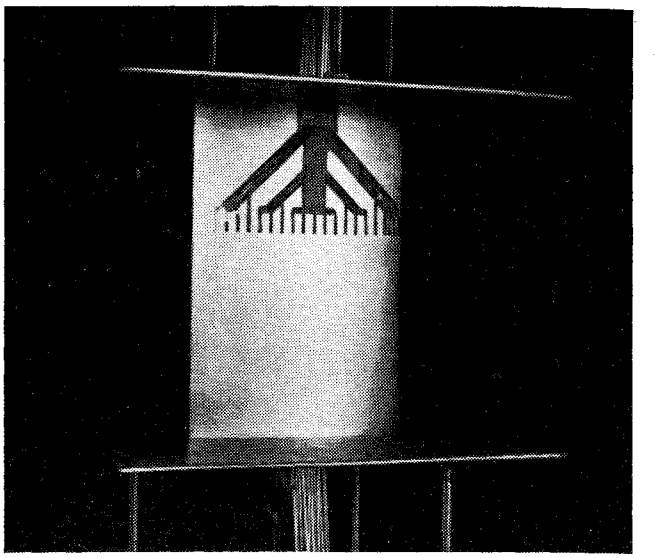

Fig. 3 Wing section with the two end plates.

tunnel flow velocities. The differences in the total and static pressures were measured with a sensitive micromanometer.

The variation of flow angle in the test section of the wind tunnel was measured with a yaw probe. The flow angle is determined by connecting the two orifices across a manometer and rotating the probe until the difference between the orifices is zero.

A DISA model 55A01 constant temperature anemometer was used to measure the mean velocity and the turbulence level in the test section at various flow velocities. A miniature hot-wire probe, DISA type 55A22, was used to survey the test section. The mean velocity across the hot-wire probe is obtained from the dc bridge voltage. In order to obtain an accurate measure of this voltage, a Data Precision 2480 digital multimeter was used for the display. For the measurement of the percent of the turbulence level, the ac rms voltage is necessary and the same Data Precision 2480 meter was used for this purpose. A turbulence level of 0.2% in the test section was determined by this hot-wire probe system.

Test Conditions

The flow velocity in the test section was adjusted to investigate the static pressure distributions over the airfoil section at Reynolds numbers, based upon the freestream conditions and a chord of 4 in. of 35,400, 71,000, 125,500, and 176,500. With the existing dc motor control and pressure instrumentation, it was not possible to obtain reliable static pressure data below a Reynolds number of 35,400, which corresponds to a flow velocity of 16 ft/s in the test section.

The static pressure distributions were obtained for an angle-of-attack range of -17 to $+18$ deg for all Reynolds numbers. At the maximum negative and positive angles of attack, the airfoil section is in the poststall conditions. The model support system was rigid enough to keep the wing steady at all flow velocities and angles of attack.

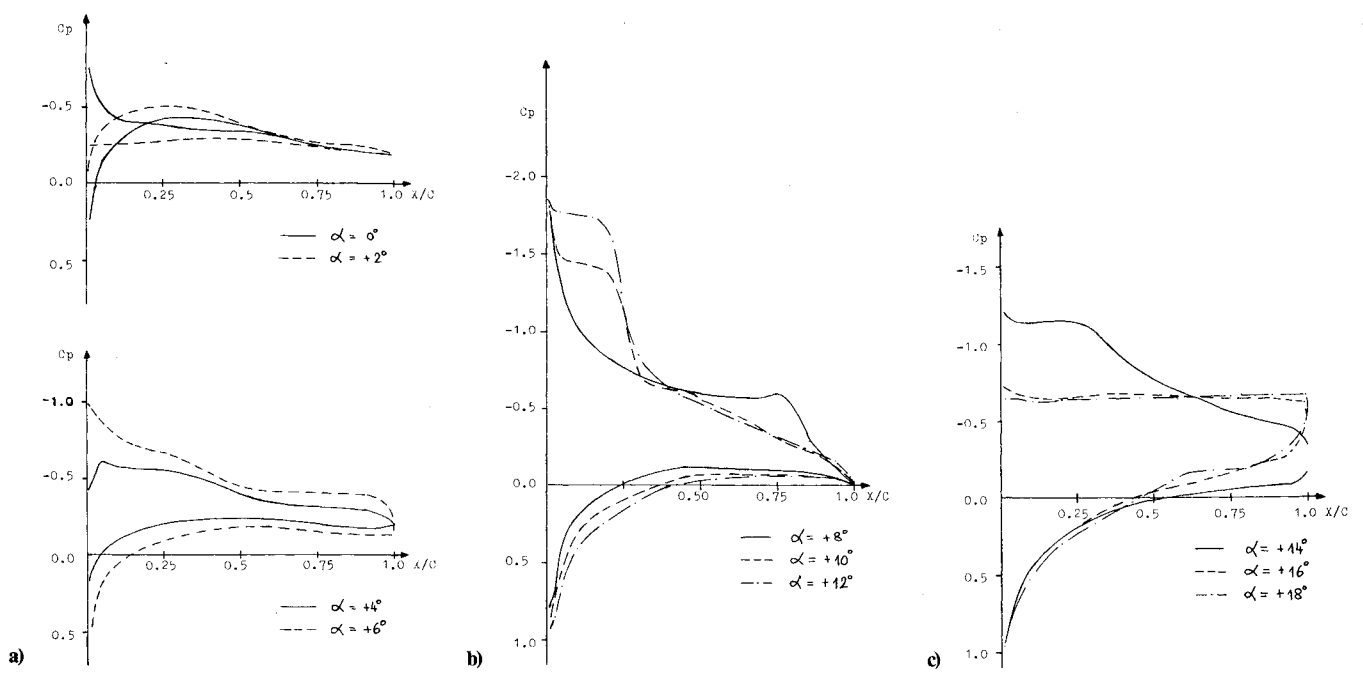

Fig. 4 Pressure distribution for $RN = 35{,}400$ and for various angles of attack, α.

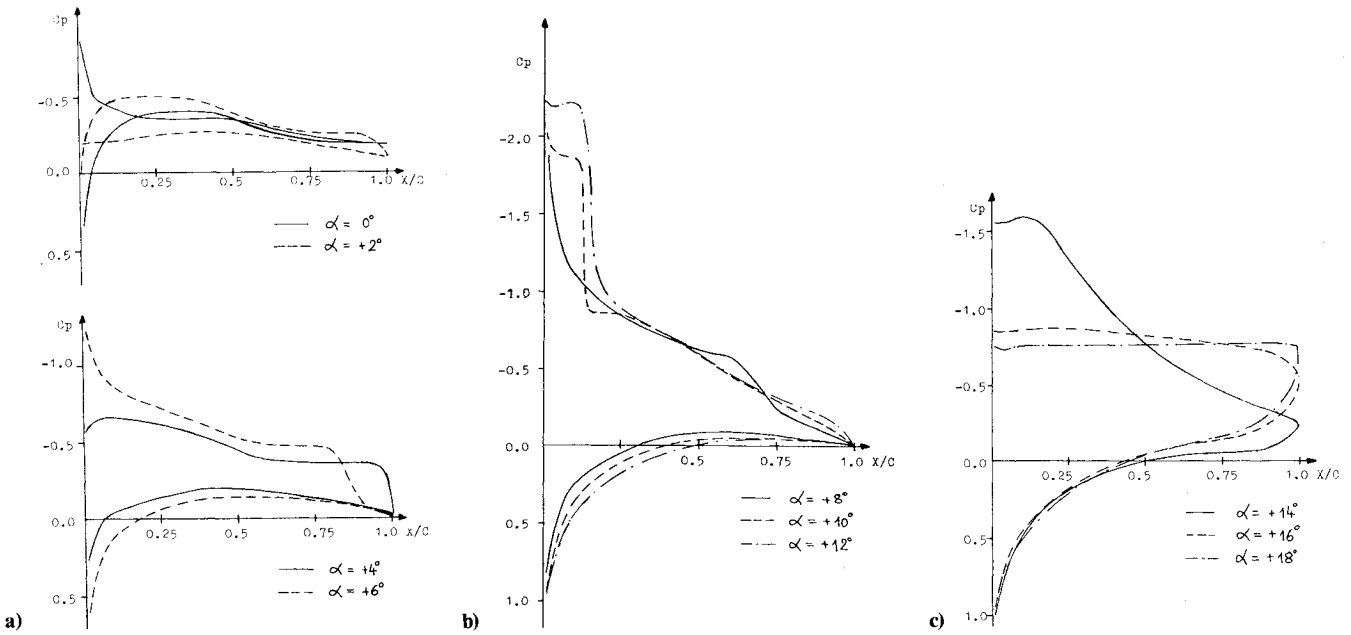

Fig. 5 Pressure distribution for $RN = 71{,}000$ and for various angles of attack, α.

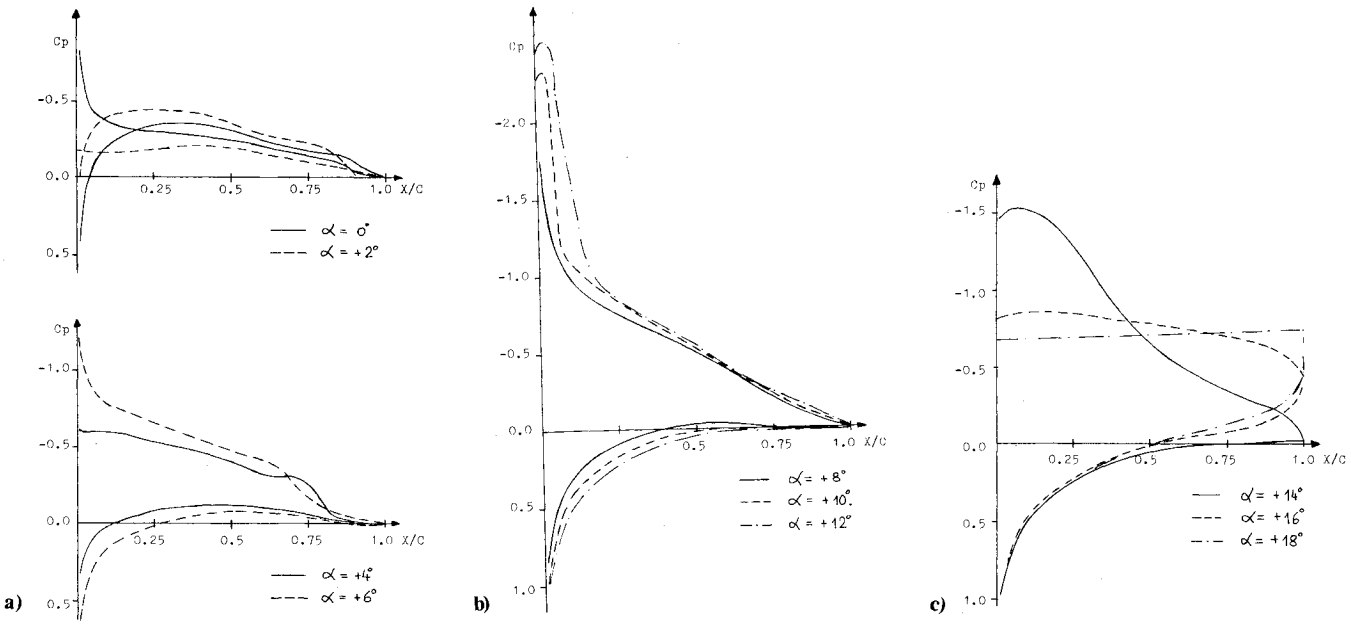

Fig. 6 Pressure distribution for $RN = 176{,}500$ and for various angles of attack, α.

Experimental Results

Pressure Distributions

The complete static pressure distributions for angles of attack of -17 to 18 deg and Reynolds numbers of 35,400 to 176,500 are presented in Ref. 15. In this paper, the static pressure distributions for an angle-of-attack range of 0 to 18 deg and Reynolds numbers of 35,400, 71,000, and 176,500 are presented in Figs. 4-6, respectively.

The static pressure coefficient distributions are quite similar for 0 deg angle of attack for Reynolds numbers of 35,400, 71,000, and 176,500 as shown in Figs. 4a, 5a, and 6a. But for angles of attack of $+2$ and $+4$ deg, the difference in the pressure coefficient toward the aft 50% of the chord increases with the Reynolds number. At an angle attack of $+6$ deg, the maximum negative pressure coefficient for a Reynolds number of 35,400 is -1.0, but for a Reynolds number of 71,000 and 176,500, the pressure coefficient is approximately -1.2. In addition, for this angle of attack, the pressure coefficient over the aft 25% of the chord is quite different for the three Reynolds numbers. At the Reynolds number of 176,500, the pressure coefficient is small toward the trailing edge, Fig. 6a, while at a Reynolds number of 35,400, the pressure coefficient is more negative and nearly constant over the rear 50% of the chord. This indicates that the flow is separated from approximately the 50% chord location.

The static pressure coefficient distributions for angles of attack of $+8$, $+10$, and $+12$ deg and Reynolds numbers of 35,400, 71,000, and 176,500 are presented in Figs. 4b, 5b, and 6b, respectively. Over the forward 50% of the chord at an

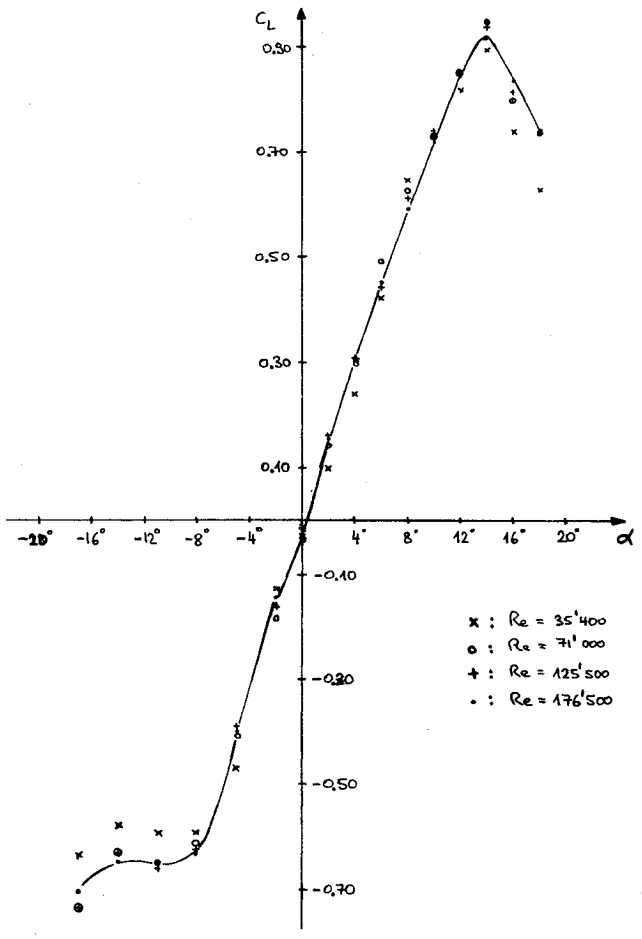

Fig. 7 Lift coefficient as functions of angle of attack and Reynolds number.

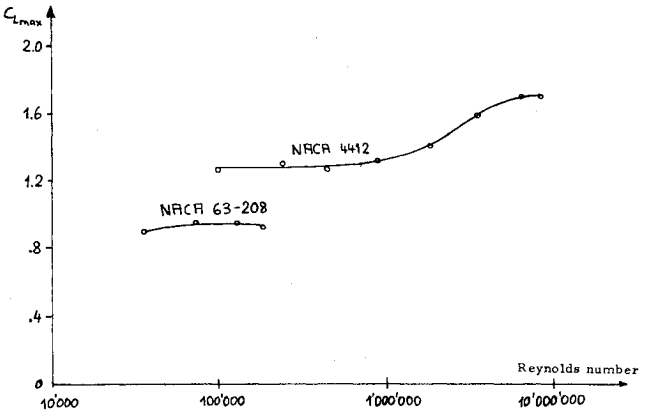

Fig. 8 Maximum lift coefficient for two airfoil sections.

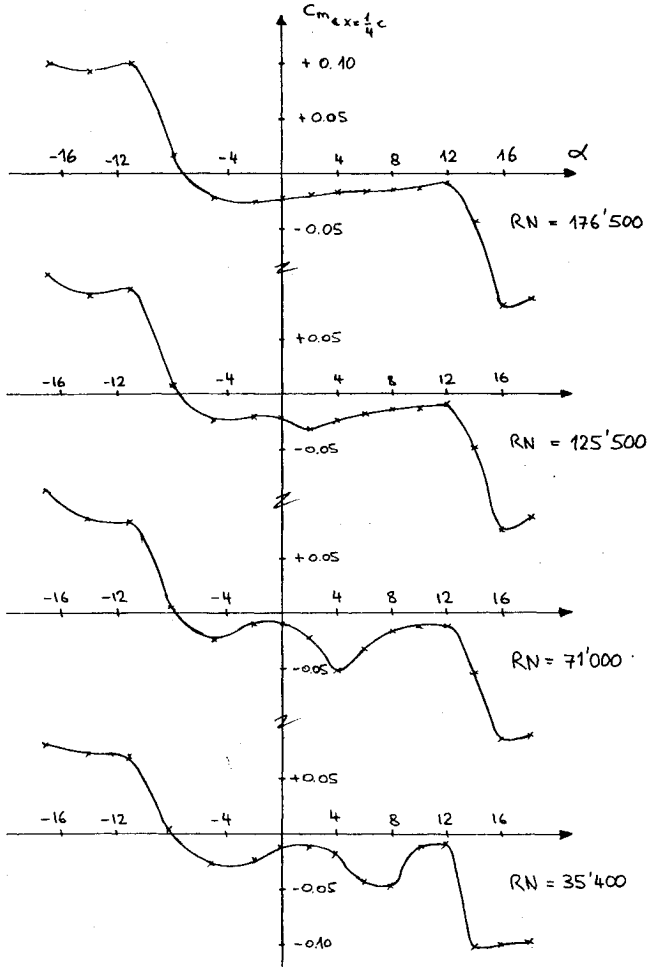

Fig. 9 Pitching moment coefficient as functions of angle of attack and Reynolds number.

angle of attack of +8 deg the pressure coefficient distributions over the chord are nearly the same for the three Reynolds numbers. But over the aft portion of the airfoil, the pressure coefficient distributions are quite different, because of the dependence of the flow separation on the Reynolds number. For +10 and +12 deg angles of attack, the laminar separated flow region, indicated by the nearly constant negative pressure coefficient over the forward 20% of the chord, decreases with the Reynolds number as shown in Figs. 4a, 5b, and 6b. But the maximum velocity near the leading edge, indicated by the maximum negative pressure coefficient, increases with the Reynolds number. The pressure coefficient is approximately −1.8 for an angle of attack of +12 deg and Reynolds number of 35,400 and increases to approximately −2.5 at a Reynolds number of 176,500.

The static pressure coefficient distributions for angles of attack of +14, +16, and +18 deg are presented in Figs. 4c, 5c, and 6c for Reynolds numbers of 35,400, 71,000, and 176,500, respectively. At a Reynolds number of 35,400 and angle of attack of +14 deg the pressure distribution indicates a separation bubble over the initial 25% of the chord with a pressure coefficient of approximately −1.2. But at Reynolds numbers of 71,000 and 176,500, the separation bubble extends over the initial 10% of the chord with a maximum pressure coefficient of approximately −1.5. For angles of attack of +16 and +18 deg the pressure distributions indicate that the flow separates at the leading edge for all Reynolds numbers. The flow over the airfoil is in the deep-stall condition.

Lift Coefficient

By integrating the static pressure coefficient distribution curves, the lift coefficient C_L was determined for angles of attack of −17 to +18 deg and Reynolds numbers of 35,400, 71,000, 125,000, and 176,500 and the results are presented in Fig. 7. The angle of attack of the model in the test section was measured accurately with a large protractor arrangement. There was a slight error in aligning the zero angle of attack of the model as indicated by the slight positive angle of attack for zero-lift coefficient for the airfoil with slight camber. Due to this camber the variation of the negative-lift coefficient near stall with angle of attack is different than for the positive stall as shown in the figure. The positive stall occurs at an angle of +14 deg for all Reynolds numbers, and the lift coefficient decreases rather rapidly at angles of attack of +16 and +18 deg. The maximum lift coefficient $C_{L_{max}}$ is approximately 0.9, which is a low value because of the relatively small leading-edge radius, Fig. 2, and low Reynolds number.

In Fig. 8 a comparison of the $C_{L_{max}}$ as a function of the Reynolds number for the present NACA 63-208 and the NACA 4412 (Ref. 12) is presented. For the 4412 airfoil section the maximum lift coefficient is approximately 1.2 over a Reynolds number range of 10^5 to 10^6, and the maximum-lift coefficient increases to 1.7 at a Reynolds number of 10^7.

Pitching Moment Coefficient

The static pressure coefficient distributions were integrated to obtain the pitching moment coefficients about the 25% chord position, and the results are presented in Fig. 9 as functions of the angle of attack and Reynolds number. For high Reynolds numbers the pitching moment coefficient is nearly constant over an angle-of-attack range of -4 to $+12$ deg, and increases drastically as stall is approached. At low Reynolds numbers the pitching moment is not constant over a range of angle of attack of -4 to $+12$ deg, but fluctuates in magnitude.

Discussion of Results

For angles of attack of 0 and $+2$ deg the static pressure coefficient distributions were nearly identical for the Reynolds number range of 35,400 to 176,500. But for angles of attack range of $+4$ to $+8$ deg, a laminar boundary layer separation occurs near the trailing edge of the airfoil and moves forward with increasing angle of attack and also with increasing Reynolds number. The pressure drop at the separation point is very sharp at low Reynolds number, however, at higher Reynolds numbers this drop becomes smooth and at Reynolds number of 176,500 is nearly imperceptible.

For angles of attack of $+10$ and $+12$ deg, it seems that two flow separations occur. The first separation is due to the formation of a bubble at the leading edge as discussed in Ref. 14. The length of the separation bubble is larger at lower Reynolds numbers. The second separation is the flow separating from the airfoil for the stalled-flow condition.

The static pressure coefficient distributions are quite similar for angles of attack of $+16$ and $+18$ deg for all Reynolds numbers. The maximum-lift coefficient of 0.9 occurred at an angle of attack of $+14$ deg. Thus, these angles are situated in the post-stalled condition for this airfoil section.

By integrating the static pressure coefficient distribution curves, the lift coefficient was obtained, and for a constant angle of attack the lift coefficient is nearly independent of the test range of the Reynolds numbers as shown in Fig. 7. The maximum lift coefficient was only 0.9 for all Reynolds numbers because of the relatively small leading-edge radius for the NACA 63-208 airfoil. At a Reynolds number of 10^5 the maximum lift coefficient for the NACA 4412 airfoil is nearly 25% greater as shown in Fig. 8. This airfoil section is thicker with larger leading-edge radius and larger camber than the NACA 63-208 airfoil.

The static pressure coefficient distributions are quite different for the range of Reynolds number of 35,400 to 176,500, but the lift coefficient at a given angle of attack is nearly the same. Thus, the variation of the pitching moment coefficient about the 25% chord location with angle of attack is strongly dependent on the Reynolds number as shown in Fig. 9. This aerodynamic characteristic for the NACA 63-208 airfoil section at low Reynolds numbers will affect the control and stability characteristics of gliders, remotely piloted vehicles, and low-speed airplanes operating at low Reynolds number flight conditions.

Conclusions

The low-speed wind tunnel with a freestream turbulence level of about 0.2% was suitable for obtaining the detailed static pressure distributions over the upper and lower surfaces for the NACA 63-208 airfoil section with end plates over a range of Reynolds numbers of 35,400 and 176,500 and angles of attack of -17 to $+18$ deg.

The static pressure distribution is independent of the low Reynolds numbers for low angles of attack less than $+2$ deg and for all angles of attack greater than $+14$ deg in the post-stalled condition. For all other angles of attack, the pressure distribution is strongly dependent on the Reynolds number.

The variation of the lift coefficient with angle of attack for different Reynolds numbers is nearly the same within the experimental accuracy, but the pressure distributions are quite different for angles of attack less than the stall angle. A maximum lift coefficient of approximately 0.9 exists for all Reynolds numbers at an angle of attack of $+14$ deg.

The pitching moment coefficient is nearly constant over an angle-of-attack range of -4 to $+12$ deg for high Reynolds numbers. At low Reynolds numbers the pitching moment is not constant over an angle-of-attack range of -4 to $+12$ deg but fluctuates in magnitude with the angle of attack.

References

[1] McGhee, R.J. and Beasley, W.D., "Low Speed Aerodynamic Characteristics of a 17 Percent Thick Airfoil Section, Designed for General Aviation Applications," NASA TN-D 7428, Dec. 1973.

[2] Beasley, W.D. and McGhee, R.J., "Low Speed Aerodynamic Characteristics of Airfoil Sections with Rounded Trailing Edges in Forward and Reverse Flow," NASA TM-X-3060, Sept. 1974.

[3] Sivier, K.R., Ormsbee, A.J., and Awker, R.W., "Low Speed Aerodynamic Characteristics of a 13.1 Percent Thick, High-Lift Airfoil," NASA CR-153937, April 1974.

[4] McCullough, G.B. and Gault, D.E., "Examples of Three Respective Types of Airfoil-Section Stall at Low Speed," NACA TN-2502, Sept. 1951.

[5] McCullough, G.B., "The Effect of Reynolds Numbers on the Stalling Characteristics and Pressure Distributions of Four Moderately Thin Airfoil Sections," NACA TN-3524, Nov. 1955.

[6] Gault, D.E., "A Correlation of Low-Speed, Airfoil Section Stalling Characteristics with Reynolds Number and Airfoil Geometry," NACA TN-3963, March 1957.

[7] Von Doenhoff, A.E. and Tetervin, N., "Investigation of the Variation of Lift Coefficient with Reynolds Number at a Moderate Angle of Attack on a Low-Drag Airfoil," NACA WRL-661, Nov. 1942.

[8] Loffin, L.K. and Potent, M.I., "Aerodynamic Characteristics of Several NACA Airfoil Sections at Seven Reynolds Numbers from 0.7 to 9×10^6," NACA RML8B02, May 1948.

[9] Eastman, J. and Sherman, A., "Airfoil Section Characteristics as Affected by Variations of the Reynolds Number," NACA TR 586, 1937.

[10] Krasilschikou, J. and Volkov, H., "Scale Effect on C_L for Reynolds Number Range of 5×10^4 to 3×10^5," Trans. Center, Aero-Hydrodynamics Institute, Moscow, No. 254, 1936.

[11] Kelling, F.H., "Experimental Investigation of a High-Lift Low-Drag Airfoil," ARC-CP-1187, 1971.

[12] Pinkerton, R.M., "The Variation with Reynolds Number of Pressure Distribution over an Airfoil Section," NACA Rept. No. 613, 1938.

[13] Nakamura, Y., Isogai, K., and Ejiri, H., "Stalling Characteristics of the NACA 0012 Airfoil Section at Low Reynolds Numbers," National Aerospace Laboratory of Japan, TR-181, June 1969.

[14] Tani, I., "Low-Speed Flows Involving Bubble Separations," *Progress in Aeronautical Sciences*, No. 5, Dec. 1964.

[15] Cuche, D.E., "Low Speed Wind Tunnel Calibration and Low Reynolds Number Aerodynamic Characteristics of the NACA 63-208 Airfoil," A Thesis submitted to the Graduate Faculty of Rensselaer Polytechnic Institute in Troy, N.Y., in partial fulfillment of the requirements for the Degree of Master of Science, April 1979.